Model reduction for molecular diffusion in nanoporous media

Gastón A. González ,[1] Ruben A. Fritz,[1] Yamil J. Colón,[2] and Felipe Herrera[1,3,*]

[1]*Department of Physics, Universidad de Santiago de Chile, Avenida Victor Jara 3493, Santiago, Chile*
[2]*Department of Chemical and Biomolecular Engineering, University of Notre Dame, Indiana, USA*
[3]*Millennium Institute for Research in Optics, Concepción, Chile*

Porous materials are widely used for applications in gas storage and separation. The diffusive properties of a variety of gases in porous media can be modeled using molecular dynamics simulations that can be computationally demanding depending on the pore geometry, complexity, and amount of gas adsorbed. We explore a dimensionality reduction approach for estimating the self-diffusion coefficient of gases in simple pores using Langevin dynamics, such that the three-dimensional (3D) atomistic interactions that determine the diffusion properties of realistic systems can be reduced to an effective one-dimensional (1D) diffusion problem along the pore axis. We demonstrate the approach by modeling the transport of nitrogen molecules in single-walled carbon nanotubes of different radii, showing that 1D Langevin models can be parametrized with a few single-particle 3D atomistic simulations. The reduced 1D model predicts accurate diffusion coefficients over a broad range of temperatures and gas densities. Our work paves the way for studying the diffusion process of more general porous materials such as zeolites or metal-organics frameworks with effective models of reduced complexity.

I. INTRODUCTION

The simulation of gas diffusion in nanoporous solid-state materials is important for applications such as gas filtering, separation, and storage [1–5]. The self-diffusion coefficient of a gas in a porous medium is an essential physical quantity that characterizes mass transfer and is a relevant parameter for designing industrial separation processes [6], diffusion of gas mixtures [4], and the selectivity of gas separation techniques [3,7–10]. The diffusive properties of gases in porous media are ultimately related to the short- and long-range interaction potentials between gas particles and between gas molecules and the condensed-phase environment [11].

The growing interest in estimating the diffusive properties of target gases in porous materials reported in public databases [5] has stimulated the search for methods to accelerate large scale screening efforts based on fully atomistic simulations, which in general are computationally demanding [8,12,13]. Acceleration strategies based on machine learning are promising because training sets with acceptable predictive power can be constructed with a smaller number of calculations than an exhaustive database search [14,15]. An alternative acceleration strategy would be to develop generalizable physics-based models that are sufficiently accurate for ranking materials based on their transport properties, but at a much lower cost than atomistic simulations.

In this context, we study the dimensionality reduction capabilities of one-dimensional (1D) Langevin dynamics for modeling gas diffusion inside carbon nanotubes at different temperatures. The predictions of the reduced model are compared to the three-dimensional (3D) molecular dynamics (MD) simulations. For concreteness, we consider the transport of molecular nitrogen in single-walled carbon nanotubes (CNTs) and obtain self-diffusion coefficients with 1D Langevin dynamics for different nanotube radii, temperatures, and gas densities. We show that it is possible to construct effective 1D pore potentials and model parameters that can reproduce the diffusive 3D transport behavior over a broad range of conditions. The proposed parametrization scheme could be extended to other porous materials such as zeolites and metal-organic frameworks.

The rest of the article is organized as follows: Section II describes the theoretical methodology and the settings for the atomistic molecular dynamics simulations. In Sec. III we discuss the results obtained for the diffusion constant of nitrogen in carbon nanotubes, comparing the predictions of the reduced 1D Langevin model, 3D molecular dynamics simulations, and the Lifson-Jackson formula from Brownian motion theory. In Sec. IV, we suggest possible applications and generalization strategies.

II. METHODOLOGY

A. Stochastic Langevin dynamics

The stochastic motion of Brownian particles can be described by a Langevin equation [16], which for a 1D system of N particles with trajectories $z^{(\alpha)}(t)$ can be written as

$$\dot{p}^{(\alpha)}(t) = -\frac{\partial V(z^N(t))}{\partial z^{(\alpha)}} - \gamma^{(\alpha)} p^{(\alpha)}(t) + \xi^{(\alpha)}(t)\bigg|_{\alpha=1,2,\dots,N},$$

$$(1)$$

where α is the particle index, p is momentum, V is the total potential, and $z^{(\alpha)}$ the position of the αth particle. The

————
*felipe.herrera.u@usach.cl

interaction of particle α with a large ensemble of bath particles is effectively taken into account by introducing the momentum loss (dissipation) term proportional to the damping parameter γ and a random momentum kick given by the random process $\xi(t)$, which induces energy fluctuation. These terms together take into account the multiples collisions of the system (Brownian) particle with the reservoir [1,16]. The random momentum kick has zero bias, i.e., $\langle \xi^{(\alpha)} \rangle = 0$ and its autocorrelation function is given by

$$\langle \xi^{(\alpha)}(0)\xi^{(\beta)}(\tau) \rangle = 2\delta(\tau)\delta_{\alpha\beta}\, m^{(\alpha)}\gamma^{(\alpha)}\, k_{\mathrm{B}}T, \quad (2)$$

where m is the particle mass, k_{B} is the Boltzmann constant, T is temperature, $\delta(t)$ is the Dirac delta function and $\delta_{\alpha\beta}$ is a Kronecker delta. In other words, momentum fluctuations are Markovian in time and proportional to the thermal energy $k_{\mathrm{B}}T$.

We solve Eq. (1) numerically for a system of N particles using the impulsive Langevin leapfrog algorithm [1], which is a modification of the classical Verlet algorithm that involves an intermediate velocity correction at each time step of the form

$$\Delta v^{(\alpha)} = \dot{v}^{(\alpha)}h - \gamma^{(\alpha)}v^{(\alpha)}(t)h + \sqrt{2k_{\mathrm{B}}T\gamma h/m^{(\alpha)}}\,\xi, \quad (3)$$

where $v^{(\alpha)}$ and $\dot{v}^{(\alpha)}$ are the velocity and acceleration of the αth particle, and h is the time step of the simulation. For a free Brownian particle at thermal equilibrium, the damping coefficient γ can be obtained from the Einstein relation [1]

$$D_0 = \frac{k_{\mathrm{B}}T}{m\gamma}, \quad (4)$$

where D_0 is the free-particle diffusion coefficient. In this work, the damping parameter γ encodes the interaction of gas molecules with the carbon nanotube walls.

B. Diffusion from mean squared displacements

We calculate the self-diffusion coefficient D_s using the mean squared displacement (MSD) method from the simulated particle trajectories. For a trajectory composed of cartesian vectors $\vec{r}_i = (x_i, y_i, z_i)$ at times t_i, the MSD can be calculated as [17]

$$\mathrm{MSD}(\tau = nh) = \frac{1}{M-n}\sum_{i=1}^{M-n}(\vec{r}_{i+n} - \vec{r}_i)^2, \quad (5)$$

which uses all available offsets τ of a given duration nh with n the offset step. The advantage of this definition is that the number of such displacements is $M - n$ and therefore it is large for small n, resulting in well-averaged MSD values. MSD is related to the self-diffusion coefficient by the expression [18]

$$\mathrm{MSD} = 2aD_s\tau, \quad (6)$$

where a is the system dimensionality ($a = 1$ for 1D, $a = 3$ for 3D). By solving Eq. (1) for all the particles in the system at fixed temperature and density, we calculate MSD from Eq. (5) and obtain D_s from the slope of a linear fit plot of Eq. (6) using the least-squares method.

For short simulation times, particle transport is dominated by the initial condition and the absence of intermolecular interactions (ballistic regime). After equilibration is reached though multiple collisions, the linear scaling of MSD with time is established (diffusive regime). Several methods have been proposed to analyze trajectories with coexisting transport regimes [19]. In our work, the diffusive regime is established when a log-log plot of MSD vs τ, averaged over particles and simulation replicas, has unit slope.

C. Lifson-Jackson model for 1D diffusion

The Lifson-Jackson formula is an analytical expression, first derived in Ref. [20], for the diffusion coefficient of a periodic 1D potential in terms of the potential depth. The periodic nature of a pristine carbon nanotube potential along its axis allows us to use this theory directly at different temperatures. For a periodic potential $V(z)$ with period L, the Lifson-Jackson diffusion coefficient can be written as [20–22]

$$D_0'(T) = \frac{D_0(T)L^2}{\left[\int_{-L/2}^{L/2} e^{-\frac{V(z)}{k_{\mathrm{B}}T}}dz\right]\left[\int_{-L/2}^{L/2} e^{\frac{V(z)}{k_{\mathrm{B}}T}}dz\right]}, \quad (7)$$

where D_0 is the free-particle diffusion coefficient from Eq. (4). For a sinusoidal potential $V(z) = A\sin(az)$ with depth A and period $a/2\pi$, the integrals in the denominator can be solved analytically to give

$$D_0'(T) = \frac{D_0(T)}{I_0^2(z)}, \quad (8)$$

where $I_n(z)$ is a modified Bessel function of the first kind and $z = A/k_{\mathrm{B}}T$. Equation (8) shows that, for sinusoidal potentials, self-diffusion is determined by the ratio between the depth of the potential and the thermal energy, independent of the lattice period. D_0' reduces to the free-particle limit at high temperatures, and asymptotically vanishes at low temperatures, as inferred from the asymptotic forms $I_0(z \to 0) \sim 1$ and $I_0(z \to \infty) \sim \infty$.

D. Molecular nitrogen in carbon nanotubes

Single-walled carbon nanotubes (SWNTs) are cylinders composed of a single wrapped graphene sheet. They are completely described, except for their length, by the notation (n, m) which refers to the direction in which the graphene sheet was rolled [23]. The index n is directly related with the nanotube radius. The self-diffusion of molecular nitrogen inside a carbon nanotube was computed over a broad range of temperatures in the range 1–10^3 K, and a range of gas densities spanning from the single-molecule limit to pore saturation. We perform calculations using zig-zag carbon nanotubes (11,0) and (15,0), with radii 4.309 and 5.876 Å, respectively. The nanotube coordinates were obtained with a modeler software [24], for a tube length of 426.3 Å. Figure 1 shows representative radial and axial views of the nanotubes used in this work. For MD and Langevin dynamics simulations, the thermal motions of carbon atoms in the nanotubes were ignored, which does not introduce significant errors in the evaluation of gas diffusion constants. We set periodic boundary conditions, random initial locations of the gas parti-
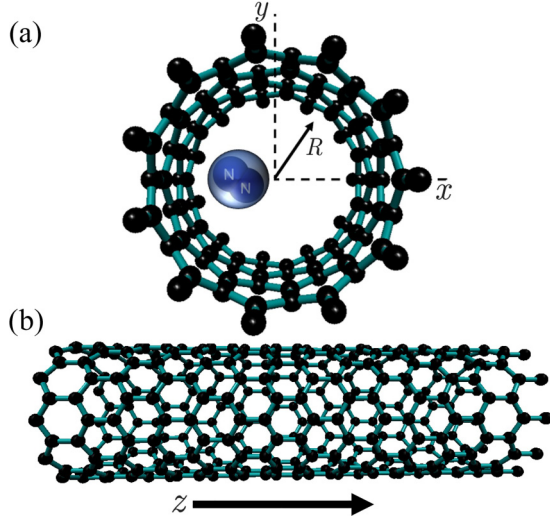
FIG. 1. (a) Radial viewpoint of the nanotube (11,0) with molecular nitrogen molecule (N_2) in its pore volume. (b) Axial viewpoint of the nanotube (11,0).
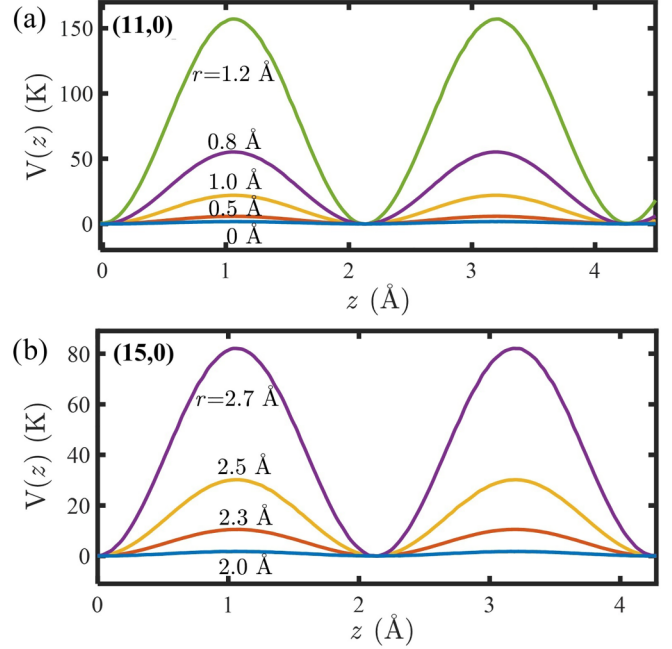

FIG. 2. (a) Axial potentials at different radii from the center of the nanotube (11,0). (b) Axial potentials for (15,0). Curves are labeled by the values of the radial coordinates. The potential is in units of kelvin.

cles, and a thermalization time of 0.5 ns in all simulations.

We model the interaction between nitrogen molecules and between nitrogen and carbon atoms in the nanotube with a Lennard-Jones potential

$$V(R) = 4\epsilon\left[\left(\frac{\sigma}{R}\right)^{12} - \left(\frac{\sigma}{R}\right)^{6}\right], \quad (9)$$

where R is the interparticle distance. The potential parameters for each particle pair in the problem are listed in Table I.

MD simulations are implemented in LAMMPS [25]. To compute 3D MSD trajectories, we adopt a non-vibrating diatomic molecule model for nitrogen, with three-dimensional rotational and translational motion inside the CNT. We use a time step $h = 1$ fs in the canonical ensemble. Each replica corresponds to a total simulation time of 5 ns. Depending on the depth of the effective axial potential experienced by a molecule in the nanotube, at very low gas densities (single particle) there is a temperature in which nitrogen molecules behave as quasifree Brownian particles, as seen from the linear scaling of the diffusion coefficient with temperature. In this regime, we assume that the Einstein relation in Eq. (4) holds and extract the effective damping parameter γ from a linear fit. For higher gas densities, nitrogen molecules are added inside the CNT with random locations and orientations. For MD simulations we define the filling ratio $\eta = \rho/\rho_0$ to quantify nitrogen density ρ relative to the tabulated density of bulk liquid nitrogen ρ_0 at the simulation temperature.

TABLE I. Lennard-Jones parameters: N-N and C-N used in LAMMPS [18]; N_2-N_2 and C-N_2 used in 1D Langevin.

	N-N	C-N	N_2-N_2	C-N_2
σ (Å)	3.32	3.36	3.63	3.52
$\epsilon/k_B(K)$	36.4	33.4	104.5	56.2

The stochastic 1D simulations were implemented in Matlab with the impulsive Langevin leapfrog algorithm [1], as mentioned previously. As input for the simulation we constructed axial potentials $V(z)$ that capture the interaction of nitrogen molecules with the CNT walls along the transport direction. In Fig. 2 we show effective axial potentials constructed for nanotubes (11,0) and (15,0) at different radial distances from the nanotube center. The potentials are periodic with a lattice constant of about 2.1 Å, which correlates with the equilibrium carbon-carbon distance in the nanotubes. At the center of the nanotubes, the depth of the axial potential becomes negligible, and is higher near the walls.

In Fig. 3 we show representative radial potentials for the nanotubes (11,0) and (15,0). The potentials feature a repulsive wall near the nanotube radius and radial barrier at the center that separates two potential minima with azimuthal symmetry. The central barrier is about 10 K high for (11,0), and 700 K for (15,0). In Figs. 3(c) and 3(d) we show the histograms of the radial positions that nitrogen molecules explore at 100 K, as obtained from 3D MD trajectories. While for (11,0) the nitrogen molecules tend to move near the center of the nanotube, for (15,0) the nitrogen molecules tend to move around the minimum of the radial potential, which has ring shape along the azimuthal coordinates. Practically no trajectories explore the nanotube center in this case.

For projecting the nitrogen molecule degrees of freedom to 1D axial motion, we replace the rotating diatomic nitrogen by a spherical mass at the position of the molecular center of mass, as illustrated in Fig. 1(a). However, the Lennard-Jones parameters in Table I do take into account the orientational dependence of the interaction potential between two nitrogen molecules and between nitrogen diatomic and carbon
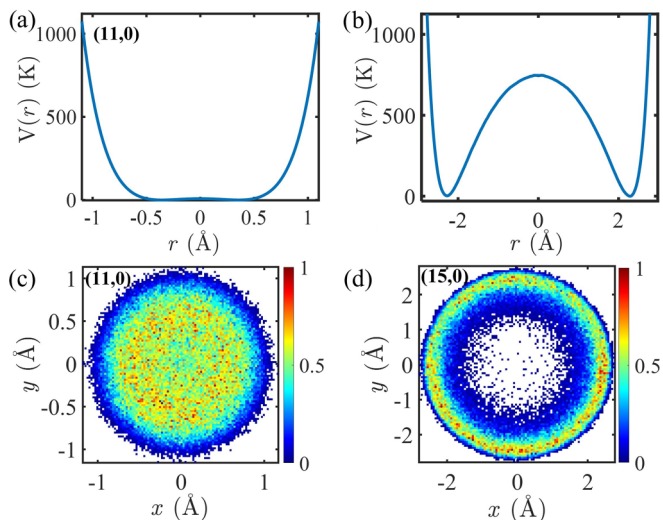
FIG. 3. (a) Effective radial potential of SWCNT(11,0) with a potential barrier in the center of approximately 10 K. (b) Effective radial potential of SWCNT(15,0) with a potential barrier in the center of approximately 700 K. (c) 2D Histogram of the nitrogen positions inside nanotube (11,0). (d) 2D Histogram of the nitrogen positions inside nanotube (15,0), at 100 K; the bar shows normalized number of counts. Blank regions correspond to spaces of the simulation box that are not explored by nitrogen molecules

atoms through a thermal averaging procedure described in the Appendix. The stochastic MSD trajectories were obtained with a damping parameter γ calibrated from a dilute nanotube MD simulation, as previously described. The 1D simulation time step is $h = 30$ fs. The total simulation time is 6.5 ns. To define a 1D filling ratio, we assume the nanotube is saturated ($\eta \approx 1$) when the number of nitrogen molecules in the simulation is equal to the ratio between the van der Waals diameter of molecular nitrogen and the length of the simulation box.

III. RESULTS AND DISCUSSION

In Fig. 4 we show the self-diffusion coefficient for a single nitrogen molecule in carbon nanotubes (11,0) and (15,0), as a function of temperature. We compare the results obtained from 3D MD simulations, 1D Langevin simulations, and the Lifson-Jackson formula. The effective axial potentials $V(z)$ for Langevin and Lifson-Jackson diffusion calculations were evaluated at a minimum of the radial potential. The Langevin damping parameter was obtained via linear fit from the MD diffusion coefficient at 100 K to give $\gamma = 7.5 \times 10^{10}$ s^{-1} for (11,0), and $\gamma = 6.0 \times 10^{10}$ s^{-1} for (15,0).

Below ~ 3 K there is essentially no diffusion in the nanotubes, because the thermal energy is lower than the corresponding axial potential depths (see Fig. 2), so particles
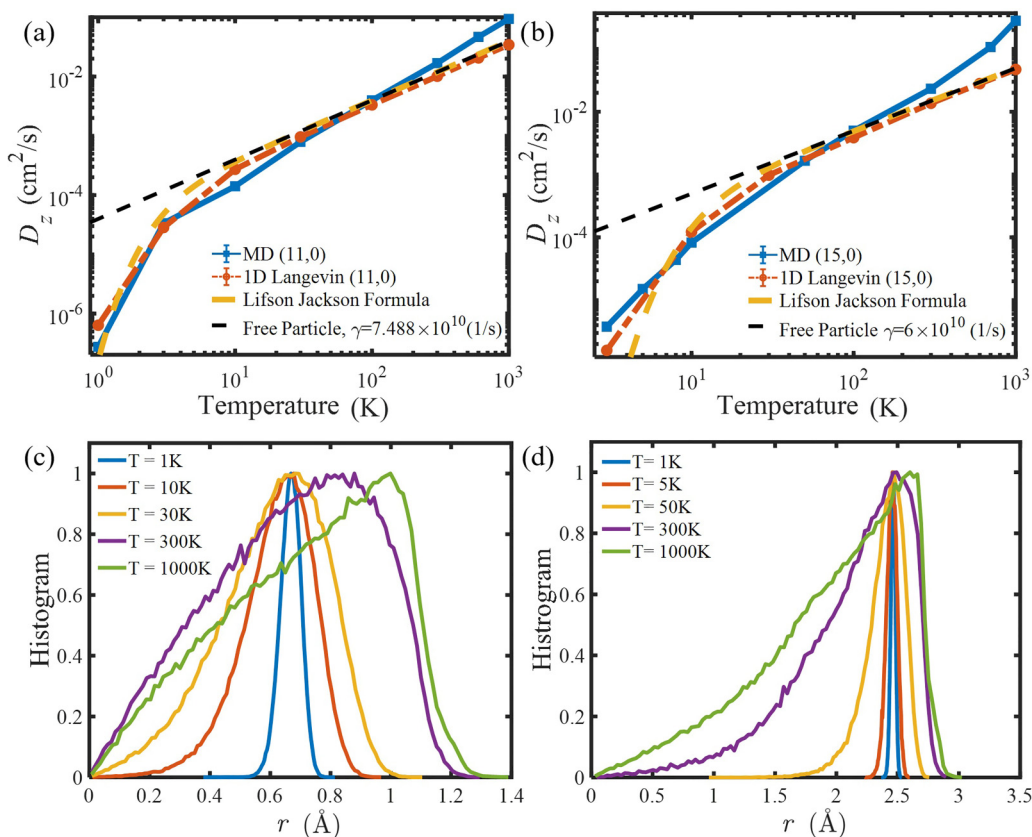

FIG. 4. (a) Single-particle diffusion vs temperature of CNT (11,0). (b) Single-particle diffusion vs temperature of CNT and (15,0). Blue: LAMMPS diffusion. Red: Langevin diffusion. Yellow: Lifson-Jackson formula. Black: free Brownian particle with $\gamma = 7.488 \times 10^{10}$ and $\gamma = 6.0 \times 10^{10}$ respectively. (c) Normalized histogram of the center of mass of each nitrogen molecule inside nanotube (11,0). (d) Normalized histogram of the center of mass of each nitrogen molecule inside nanotube (15,0). Curves are labeled by the value of the temperature.
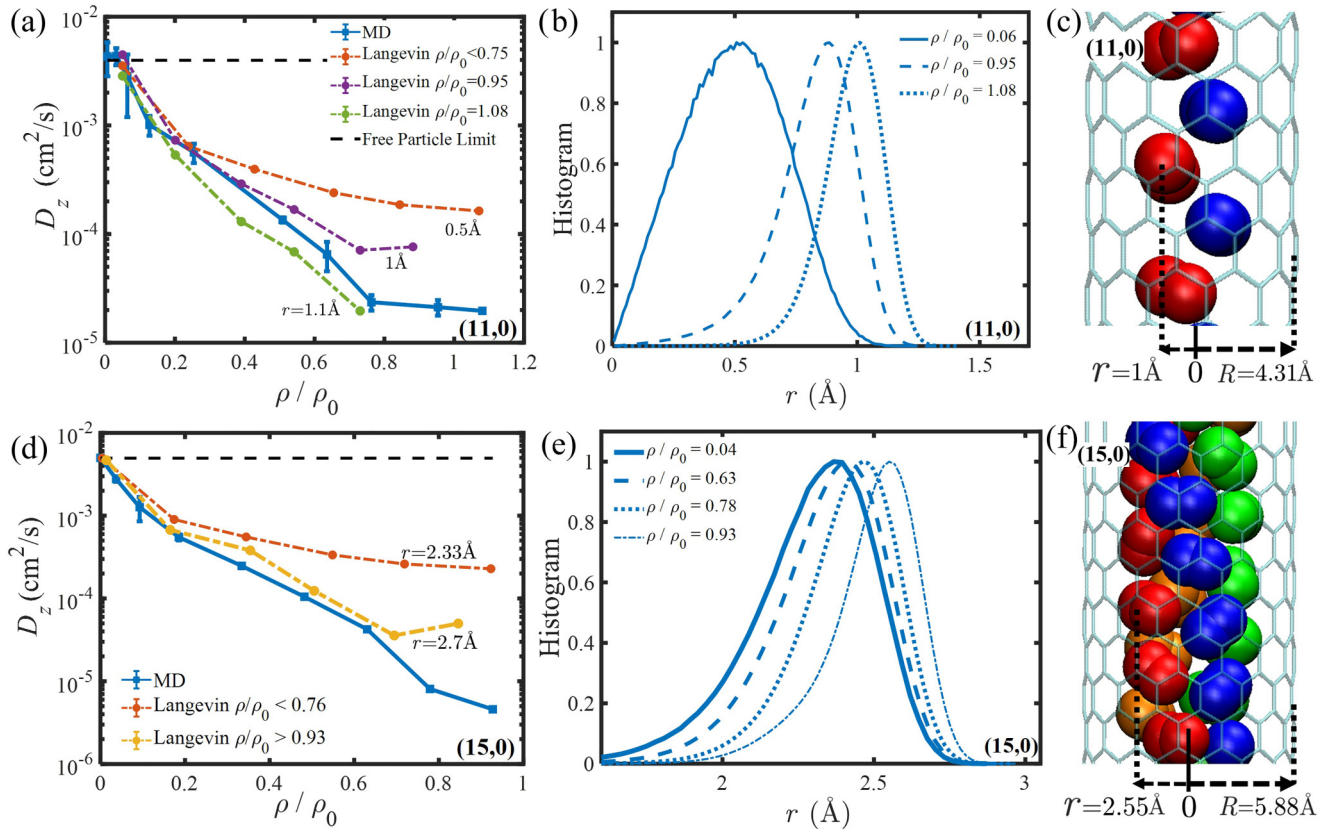
FIG. 5. (a) Diffusion vs density (11,0) at 100 K. Blue: MD. Red, green, and purple: Langevin diffusion with different depths of axial potentials as a function of the radial distance from the center of the nanotube. Black: free particle limit according to Eq. (4) with $\gamma = 7.488 \times 10^{10}$. (b) Histogram of the radial positions of nitrogen molecules at different densities in MD of CNT (11,0). (c) Graphical modeling of the nitrogen molecules inside the (11,0) nanotube at the relative saturation density $\rho/\rho_0 = 1.08$, made with VMD [26] (d) Diffusion vs density (15,0) at 100 K. Blue: MD. Red, green, and purple: Langevin diffusion with different depths of axial potentials as a function of the radial distance from the center of the nanotube. Black: free particle limit according to Eq. (4) with $\gamma = 6.0 \times 10^{10}$. (e) Histogram of the radial positions of nitrogen molecules at different densities in MD of CNT (15,0). (f) Graphical modeling of the nitrogen molecules inside the (15,0) nanotube at at the relative saturation density $\rho/\rho_0 = 0.93$, made with VMD [26]

become trapped in the axial potential. At higher temperatures, the MSD trajectory analysis gives a diffusive regime with a log-log slope of 1 ± 0.15 [18], from which we obtain converged diffusion coefficients.

As the temperature increases, all methods capture a crossover between particle trapping and diffusion around 10 K, beyond which the diffusion constant scales linearly with temperature, as expected from Eq. (4) for quasifree Brownian motion. The self-diffusion coefficients for 1D Langevin and Lifson-Jackson formulas coincide in the entire range of temperatures studied. However, while the orders of magnitude are the same, the 3D diffusion coefficients obtained with MD are consistently greater. The similarity in self-diffusion coefficients of the 1D Langevin and Lifson-Jackson formulas can be explained by the fact that both methods use the same one-dimensional axial potential as input data. In addition, at high temperatures they must converge to the value of D_0. The discrepancy between 3D and 1D results grows with temperature, as Fig. 4(b) illustrates more clearly for the wider (15,0) nanotube.

To understand this discrepancy at high temperature, in Figs. 4(c) and 4(d) we show the histograms of the radial positions of the centers of mass explored by nitrogen molecules

at different temperatures for the nanotubes (11,0) and (15,0), obtained from 3D MD trajectories. At low temperatures ($T \sim 10$ K), molecules are mostly trapped at the minima of their corresponding radial potentials. At higher temperatures ($T \sim 100$ K), particles have more energy to explore a larger fraction of the nanotube pore volume, broadening the radial distribution and displacing the most-probable radius towards the nanotube walls. This effective increase in the configuration space involved in axial transport cannot be captured by the effective 1D Langevin model, without redefining γ. However, the agreement is excellent between the dilute 1D Langevin with a single value of γ and the 3D MD simulations, over a broad range of temperatures.

In Figs. 5(a) and 5(b) we plot the nitrogen diffusion coefficient as a function of the gas filling ratio $\eta = \rho/\rho_0$ for (11,0) and (15,0) nanotubes, respectively. We compare the results obtained from 3D MD and 1D Langevin simulations at 100 K. For the 1D calculations, we approximately capture the density dependence of the effective axial molecule-nanotube axial potential by evaluating the nitrogen-nanotube axial potential at the peak of the radial distribution of MD trajectories shown in Fig. 5(b) for (11,0) and Fig. 5(e) for (15,0). For increasing molecular densities, close to saturation ($\eta > 0.90$), the radial

density of trajectories peaks closer to the pore walls. In general, both 3D and 1D simulations give diffusion coefficients that decrease monotonically with the pore occupation for the two nanotube radii considered.

Depending on the radial position used to estimate the depth of the effective axial potential $V(z)$, the Langevin calculations can approximate the atomistic 3D results reasonably well over the entire range of densities up to the saturation regime ($\eta \sim 1$). For axial potential depths below 30 K ($r < 0.8$ Å), Fig. 5(a) shows that the agreement between the 1D and 3D curves is excellent up to $\eta \approx 0.4$ for (11,0) nanotubes. At these low gas concentrations, nitrogen molecules move preferably near the center of the nanotube [see the peak at $r = 0.5$ Å in Fig. 5(b)].

At higher densities ($\eta \sim 0.8$–1.0), there is a sudden shift in radial density towards the walls of the (11,0) nanotube. This shift is due to emergence of stacked configurations between nitrogen molecules, as shown in Fig. 5(c) where the nitrogen molecules are pushed towards the walls of the nanotube finding different axial potentials. At higher densities, the Langevin simulations consistently overestimate the diffusion coefficient relative to atomistic MD, although both 1D and 3D continue to have similar qualitative behavior, reaching asymptotic saturation for $\eta \sim 1$. By evaluating the axial potential closer to the peak of the radial trajectory distribution at the corresponding density [see Fig. 5(b)], the Langevin results can be made to agree with the MD simulations over a wider range of densities with the same low-density value of γ.

For the wider (15,0) nanotube, we find similar trends when comparing 1D and 3D diffusion coefficients in Fig. 5(d). Again the agreement between MD and Langevin simulations can be improved by sampling the axial potential closer to the peak of the radial trajectory distribution at a given gas density [Fig. 5(e)]. The main qualitative difference between (11,0) and (15,0) nanotubes occurs near saturation, as the larger pore volume of (15,0) allows for more intricate stacking configurations of the nitrogen molecules, which are more difficult to capture with 1D effective models than the small-pore saturation behavior of (11,0), At different densities of nitrogen molecules, different stacking configurations are created, affecting the axial interaction potential. For example. Fig. 5(f) shows a representative quadruple "helix" configuration that nitrogen molecules adopt at high filling ratios in the (15,0) nanotube ($\eta = 0.9$). These helical structures have been reported in carbon nanotubes for nitrogen [18] and water [27].

To assess the gain in computational resources that a reduced Langevin model can potentially introduce for studying the transport properties of porous materials, we note that the density dependence of the diffusion constants in Figs. 5(a) and 5(d) can be reproduced with the 1D Langevin model from the dilute regime up to the nanotube saturation limit using, in principle, only 3 MD simulations: two low-density simulations to calibrate γ, and one additional simulation for a selected saturation level ρ/ρ_0 to calibrate the choice of the radius r (a free parameter) at which the effective axial potential $V(z, r)$ should be evaluated. These MD calculations fully parametrize the Langevin model and allow for predictions of the diffusion coefficient over a broader range of temperatures and densities than the original simulation conditions.
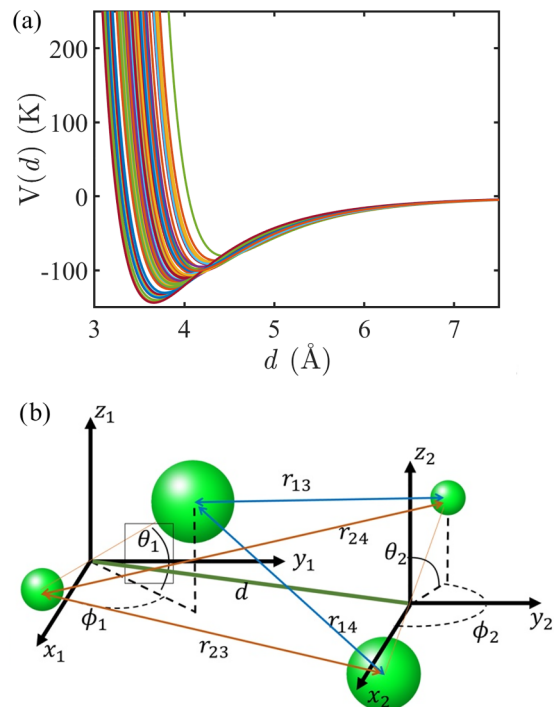

FIG. 6. (a) Interaction potentials of for a pair of nitrogen molecules considering all possible orientations. (b) Scheme of spatial coordinates for a pair of nitrogen molecules

IV. CONCLUSIONS

In this work we developed an effective one-dimensional Langevin equation model for the diffusive transport for dilute and dense molecular gases inside carbon nanotubes, as a function of tube radius and temperature. By parametrizing the Langevin model using atomistic molecular dynamics simulations over a limited range of densities and temperatures, we find that the reduced stochastic approach can accurately extrapolate the behavior of the diffusion coefficient over a broader range of temperatures and nanotube filling ratios. For higher densities closer to saturation, we show that the effective potential that drives the Langevin dynamics along the nanotube axis can be adjusted to account for the interaction between gas particles over transverse degrees of freedom, and propose criteria to obtain effective Langevin potentials and damping parameters using nitrogen transport in carbon nanotubes as an example. We envision future extensions of the proposed dimensionality reduction methodology to study diffusive transport of gases and liquids in complex nanoporous media such as metal-organic frameworks, zeolites, and structured electrodes, which could facilitate the large-scale screening of materials for applications in energy, catalysis, and gas separation.

ACKNOWLEDGMENTS

APPENDIX: EFFECTIVE INTERACTION POTENTIAL

We want to find the effective potential between the diatomic molecules of N_2 and C-N_2. If we simulate a large set of potentials of N_2-N_2 considering all possible configurations or orientations with equal probability, we obtain a wide range of potential values, as shown in Fig. 6(a). Linearly adding the interactions between each pair of molecules (r_{13}, r_{14}, r_{23}, r_{24}) for random orientations of each molecule [Fig. 6(b)] and then averaging with a Boltzman weight, it is possible to find an effective total potential at a certain temperature:

$$V(T, d) = \frac{\sum_i e^{\frac{-min(V_i(d))}{k_B T}} \times V_i(d)}{\sum_i e^{\frac{-min(V_i(d))}{k_B T}}}. \qquad (A1)$$

This effect is easily explained if we consider the effect of the spatial orientations of the N_2 molecules. At low temperatures, the possible spatial orientations experienced by the N_2 molecule are "limited." They are arranged in such a way as to minimize energy. The opposite is the case at high temperatures that experiences almost equally all possible spatial orientations, including (for example) a system of two interacting N_2 molecules arranged collinearly in space (system where energy is maximized). Replicating the previous calculation, the interaction potential between C-N_2 can be determined, we can calculate the potential as a function of the radius of the interior of the nanotube. Finally, by finding the minima of the potentials and their intersection with zero, we can determine their potential analog of Lennard-Jones; the parameters obtained are found in Table I.

[1] N. Goga, A. Rzepiela, A. De Vries, S. Marrink, and H. Berendsen, J. Chem. Theory Comput. **8**, 3637 (2012).

[2] P. A. Gordon and R. B. Saeger, Ind. Eng. Chem. Res. **38**, 4647 (1999).

[3] H. Daglar and S. Keskin, J. Phys. Chem. C **122**, 17347 (2018).

[4] R. Krishna and J. Van Baten, Ind. Eng. Chem. Res. **44**, 6939 (2005).

[5] Y. J. Colón and R. Q. Snurr, Chem. Soc. Rev. **43**, 5735 (2014).

[6] H. Liu and E. A. Macedo, J. Supercrit. Fluids **8**, 310 (1995).

[7] W. J. Koros and C. Zhang, Nat. Mater. **16**, 289 (2017).

[8] F. J. Keil, R. Krishna, and M.-O. Coppens, Rev. Chem. Eng. **16**, 71 (2000).

[9] A. Mace, N. Hedin, and A. Laaksonen, J. Phys. Chem. C **117**, 24259 (2013).

[10] Z. Gu, W. Song, Z. Yang, and R. Zhou, Phys. Chem. Chem. Phys. **20**, 30384 (2018).

[11] I. N. Tsimpanogiannis, O. A. Moultos, L. F. Franco, M. B. d. M. Spera, M. Erdős, and I. G. Economou, Mol. Simul. **45**, 425 (2019).

[12] V. Sokhan, D. Nicholson, and N. Quirke, J. Chem. Phys. **120**, 3855 (2004).

[13] Y. Pramudya, S. Bonakala, D. Antypov, P. M. Bhatt, A. Shkurenko, M. Eddaoudi, M. J. Rosseinsky, and M. S. Dyer, Phys. Chem. Chem. Phys. **22**, 23073 (2020).

[14] H. Tang, Q. Xu, M. Wang, and J. Jiang, ACS Appl. Mater. Interfaces **13**, 53454 (2021).

[15] I. B. Orhan, H. Daglar, S. Keskin, T. C. Le, and R. Babarao, ACS Appl. Mater. Interfaces **14**, 736 (2022).

[16] E. Paquet and H. L. Viktor, BioMed Res. Int. **2015**, 183918 (2015).

[17] X. Michalet, Phys. Rev. E **82**, 041914 (2010).

[18] G. Arora and S. I. Sandler, J. Chem. Phys. **124**, 084702 (2006).

[19] H. Qian, M. P. Sheetz, and E. L. Elson, Biophys. J. **60**, 910 (1991).

[20] S. Lifson and J. L. Jackson, J. Chem. Phys. **36**, 2410 (1962).

[21] P. Reimann, C. Van den Broeck, H. Linke, P. Hänggi, J. Rubi, and A. Pérez-Madrid, Phys. Rev. Lett. **87**, 010602 (2001).

[22] A. M. Berezhkovskii and L. Dagdug, J. Chem. Phys. **151**, 131102 (2019).

[23] T. Belin and F. Epron, Materials Science and Engineering: B **119**, 105 (2005).

[24] JCrystalSoft, Nanotube Modeler, 2004–2005.

[25] S. Plimpton, J. Comput. Phys. **117**, 1 (1995).

[26] W. Humphrey, A. Dalke, and K. Schulten, J. Mol. Graphics **14**, 33 (1996).

[27] W. H. Noon, K. D. Ausman, R. E. Smalley, and J. Ma, Chem. Phys. Lett. **355**, 445 (2002).